Inertia effects in TLD sloshing with perforated screens

Bernard Molin, Fabien Remy

Inertia effects in TLD sloshing with perforated screens

Bernard Molin *, Fabien Remy

Aix Marseille Université, CNRS, Centrale Marseille, IRPHE UMR 7342, 13451 Marseille cedex 13, France

Rectangular tanks equipped with perforated screens and partly filled with water have been proposed as Tuned Liquid Dampers (TLDs) to mitigate the vibratory response of slender buildings. In a previous paper (Molin & Remy 2013)an experimental campaign was reported and its results compared with a numerical model, based on linearized potential flow theory. Good agreement was generally obtained for the added mass and damping coefficients. In these experiments the screen had numerous circular openings, 4 mm in diameter, and it was assumed in the numerical model that the screen created a pressure drop proportional to the square of the relative traversing velocity. In this subsequent paper complementary experiments are described where the screen openings are increased in size, keeping constant the open-area ratio, and varied in shapes (vertical slots then circular holes). As a result of the solid parts of the screen getting larger, inertia effects come into play resulting in a shift of the resonant frequencies of the odd sloshing modes. With a proper modification of the discharge law in the numerical model, ccounting for inertia effects, good agreement is recovered between experimental and numerical hydrodynamic coefficients.

1. Introduction

In the past years a wide literature has appeared on so-called Tuned Liquid Dampers (TLDs) or Tuned Sloshing Dampers. We refer the readers to Tait (2008), Faltinsen et al. (2011a) or Crowley and Porter (2012b) where comprehensive reviews can be found. These TLDs, which serve the purpose of mitigating the wind or earthquake vibratory response of tall buildings, consist in tanks partially filled with water and equipped with damping screens. In a previous paper (Molin and Remy, 2013), experimental and numerical values of the hydrodynamic coefficients (added mass and damping) are presented for a rectangular tank with a perforated screen at mid-length. The experimental tank has a length of 0.8 m, a width of 0.5 m and the filling height is 0.32 m. The screen consists in a rigid 2 mm thick steel plate with round openings 4 mm in diameter covering 18% of the surface. In the numerical model the screen is idealized as a porous boundary where the normal flow velocity is continuous and the pressure differential Δp is related to the square of the traversing velocity (relative to the screen) V through the law

$$\Delta p = \rho \frac{1-\tau}{2\mu\tau^2} V|V|, \tag{1}$$

with ρ being the fluid density, τ the open-area ratio (or porosity) and μ a discharge coefficient taken equal to 0.5.

* Corresponding author.
E-mail addresses: bernard.molin@centrale-marseille.fr (B. Molin), fabien.remy@centrale-marseille.fr (F. Remy).

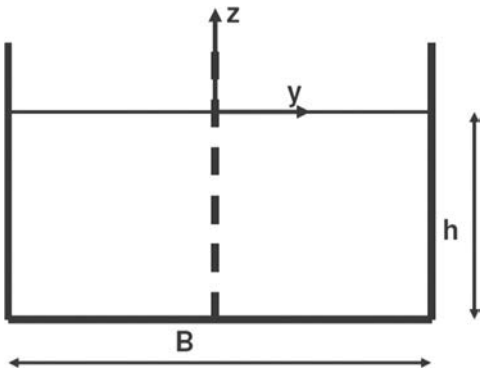

Fig. 1. Geometry.

Good agreement is reported between experimental and numerical hydrodynamic coefficients in sway and roll.

The discharge law (1) is based on previous experience of the authors with similar perforated screens (for a review see Molin, 2011). It does not account for any inertia effect. In Molin (2011), it is advocated that (1) holds in the limit when, at given porosity ratio, the number of openings goes to infinity or, equivalently, their size goes to zero. As the open and solid parts increase in size from zero, inertia effects gradually come into play. In the case of slotted screens, the inertia contribution to the pressure drop may be derived from the parent case, in acoustics, of a slot in a rectangular duct. See Mei (1983, p. 255), Bennett et al. (1992) and, more recently, Crowley and Porter (2012a,b).

It is straight-forward to incorporate an inertia term, such as proposed by Mei (1983), in (1). Note that this means that, alike in the Morison equation, the viscous and potential flow effects are separated and their interaction is disregarded. Moreover the succession of solid and open parts of the screen is still modeled as one continuous porous boundary. Results from physical tests are therefore required to ascertain the domain of validity of the numerical values obtained.

In this paper experimental results are reported where the perforated screen tested in Molin and Remy (2013) is replaced with successive arrangements of vertical slats and slots, varying their number over the width of the tank while keeping constant the open-area ratio. In a second series of tests, screens with circular openings are considered, with the number of openings being gradually decreased.

Tests are performed in forced translatory harmonic motion and the added mass and damping coefficients, derived from the force measurements, are compared with predictions from the numerical model.

2. Numerical model

2.1. Slatted screens

The geometry is described in Fig. 1. The tank is rectangular, with a length B and a water height h. The perforated screen, set at mid-length, consists in a periodic succession of vertical slats and slots, all over the width d of the tank (see Fig. 3). The thickness of the solid parts is assumed to be nil.

The tank is undergoing forced harmonic horizontal motion of frequency ω and amplitude A: $Y(t)=A\ \sin\ \omega t$.

The same numerical model as described in Molin and Remy (2013) is used, with a complementary inertia term in the discharge equation. We refer the reader to that paper for details. The problem is tackled within the framework of linearized potential flow theory, in the frequency domain (i.e. the steady-state solution is sought) through eigen-function expansions. The slotted screen is idealized as a continuous porous boundary, all over the width and height of the tank. This makes the problem two-dimensional in a plane (y,z). With the velocity potential being written as

$$\Phi(y,z,t)=\Re\left\{\varphi(y,z)\mathrm{e}^{-\mathrm{i}\,\omega t}\right\}, \tag{2}$$

the discharge law (1) at the porous wall is complemented with an inertia term and becomes

$$\mathrm{i}\,\omega(\varphi_{-}-\varphi_{+})=\frac{4}{3\pi}\frac{1-\tau}{\mu\tau^2}\|\varphi_y-A\omega\|\left(\varphi_y-A\omega\right)-\mathrm{i}\,\omega(1-\tau)^2\pi C_a(\tau)\frac{d}{4N_S}\left(\varphi_y-A\omega\right), \tag{3}$$

with φ_{-} (resp. φ_{+}) being the velocity potential on the left-hand (resp. right-hand) side of the screen, N_S the number of slots over the width d of the tank and $C_a(\tau)$ the added mass coefficient given as (Morse and Ingard, 1968; Mei, 1983; see also Molin, 2011):

$$C_a(\tau)=\frac{8}{(1-\tau)^2\pi^2}\ln\left[\frac{1}{2}\tan\frac{\pi\tau}{4}+\frac{1}{2}\cot\frac{\pi\tau}{4}\right]=-\frac{8}{(1-\tau)^2\pi^2}\ln\left[\sin\frac{\pi\tau}{2}\right]. \tag{4}$$

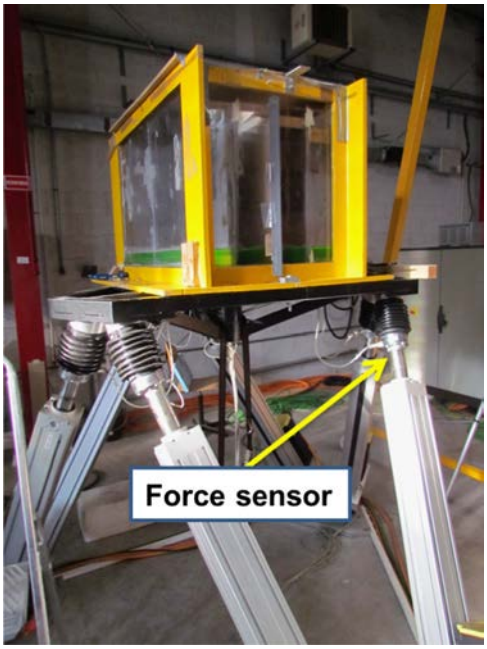

Fig. 2. The tank on ECM Mistral Hexapode.

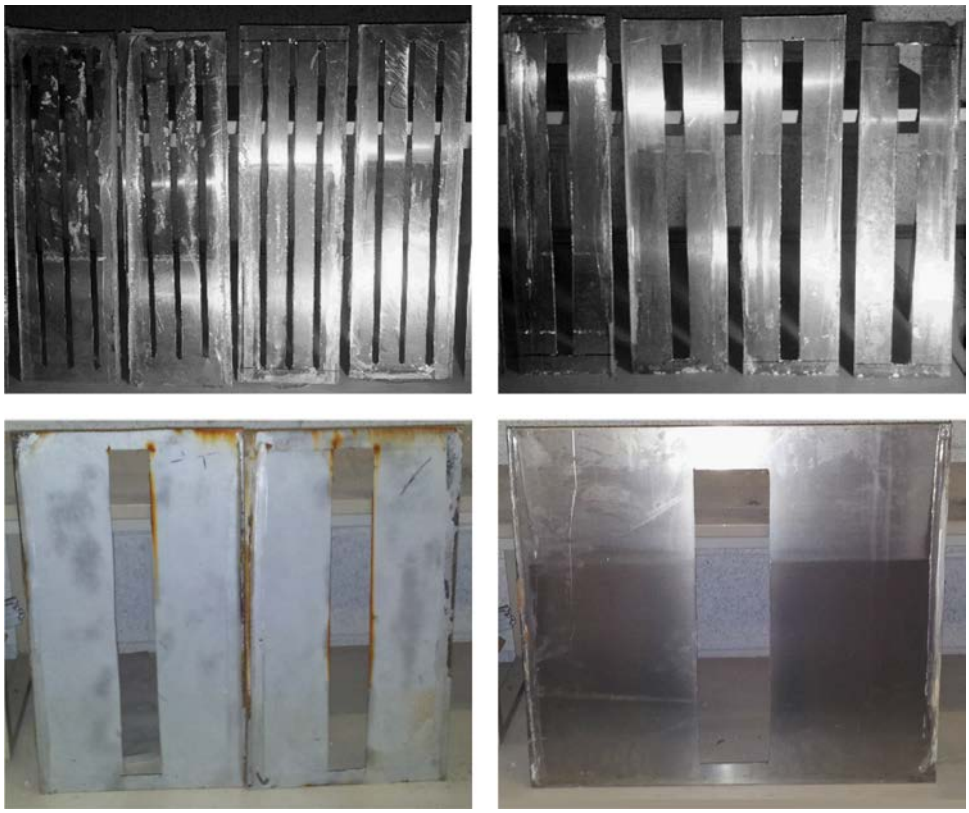

Fig. 3. Slatted screens: 12 slots (top left), 4 slots (top right), 2 slots (bottom left), 1 slot (bottom right).

The added mass coefficient C_a is here referred to an area πc^2 with c being half the slat width $c = (1-\tau)d/(2\,N_S)$. The inertia term in (3) can easily be checked to be identical with the expression given in Crowley and Porter (2012a), and also used in Bennett et al. (1992).

2.2. Circular openings

A similar approach can be applied to the case of circular openings, by reference to the case of a circular diaphragm of radius a inside a circular pipe of radius $b = a/\sqrt{\tau}$. We have not been able to find analytical or semi-analytical values for this added mass coefficient in the literature, so we have worked it out through eigen-function expansion (see Appendix).

The discharge law is now written

$$\mathrm{i}\,\omega\ (\varphi_- - \varphi_+) = \frac{4}{3\pi}\frac{1-\tau}{\mu\tau^2}\|\varphi_y - A\omega\|\left(\varphi_y - A\omega\right) - \mathrm{i}\,\omega\frac{C_a(\tau)a}{\pi\sqrt{\tau}}\left(\varphi_y - A\omega\right), \tag{5}$$

with $C_a(\tau)$ being the added mass coefficient shown in Fig. 22. Note that this added mass coefficient is referred to a mass ρb^3, with $b = a/\sqrt{\tau}$. At a porosity ration of 18%, $C_a \simeq 5.0$.

In all calculations, with the two types of openings, the discharge coefficient μ was taken equal to 0.5, alike in Molin and Remy (2013).

3. Experimental set-up

The same bench (Mistral Hexapode) and the same tank as in Molin and Remy (2013) have been used (Fig. 2). The Mistral Hexapode is equipped with force sensors that give access, after some processing, to the complete hydrodynamic torque due to the sloshing motion in the tank. Subsequent Fourier analysis yields the added mass C_a and damping C_b coefficients referred to the liquid mass ρBdh, that is the first harmonic of the hydrodynamic force in sway is written as

$$F_y = \Re\left\{\mathrm{i}\,\rho A\omega^2 Bdh\ (C_a + \mathrm{i}\,C_b)\mathrm{e}^{-\mathrm{i}\,\omega t}\right\}. \tag{6}$$

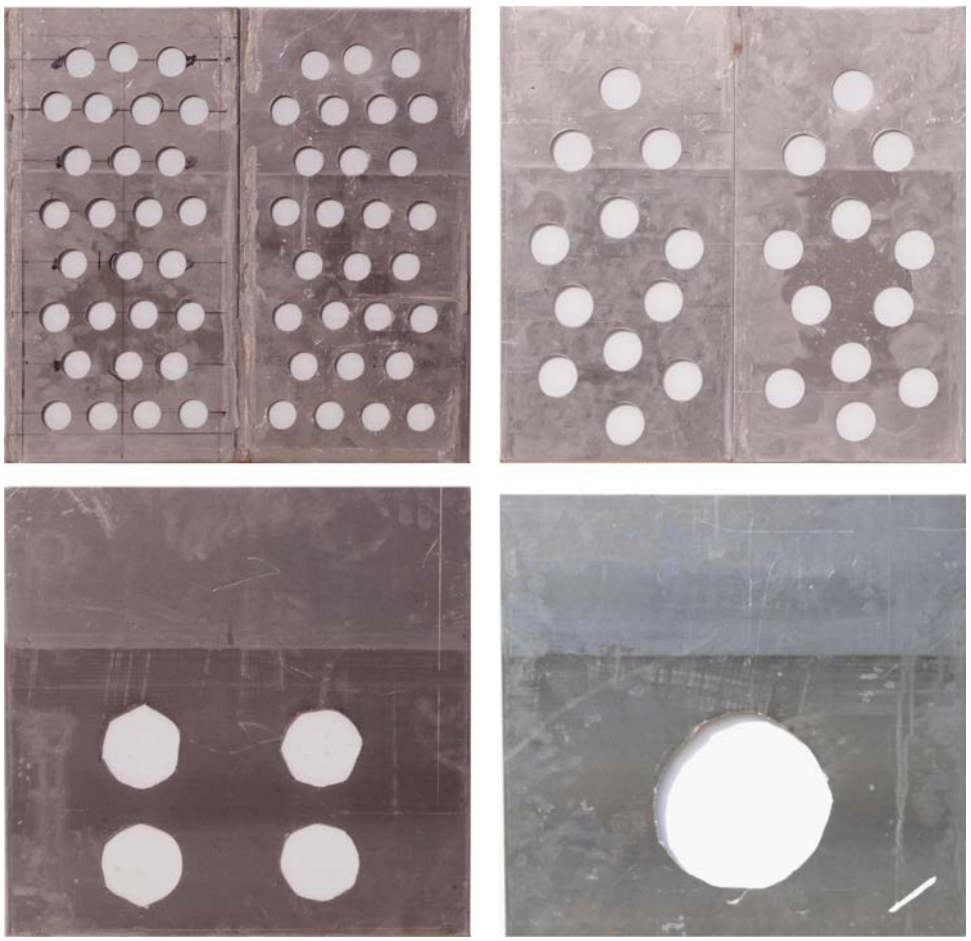

Fig. 4. Screens with circular openings: 36 holes (top left), 18 holes (top right), 4 holes (bottom left), 1 hole (bottom right).

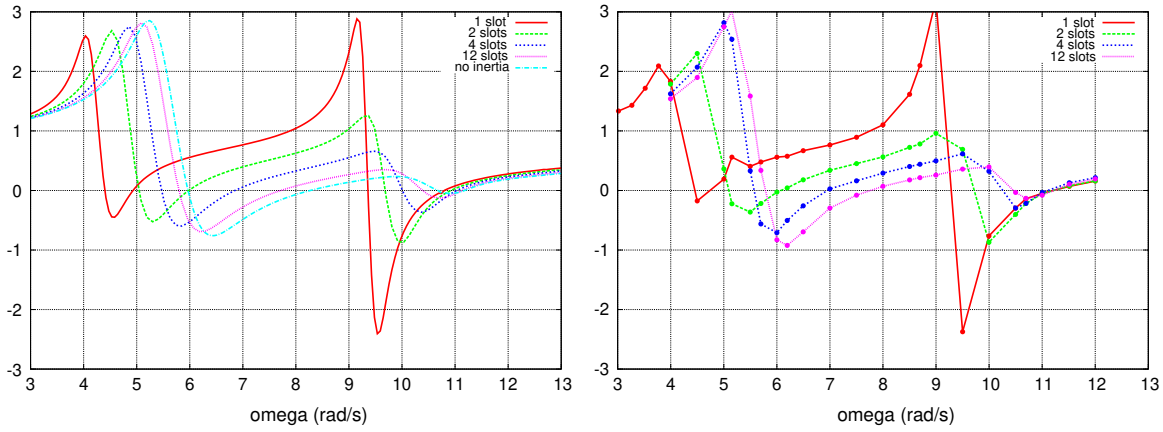

Fig. 5. Slatted screens. Added mass coefficient. Forced motion amplitude 1 mm. Calculated (left) and measured (right) values.

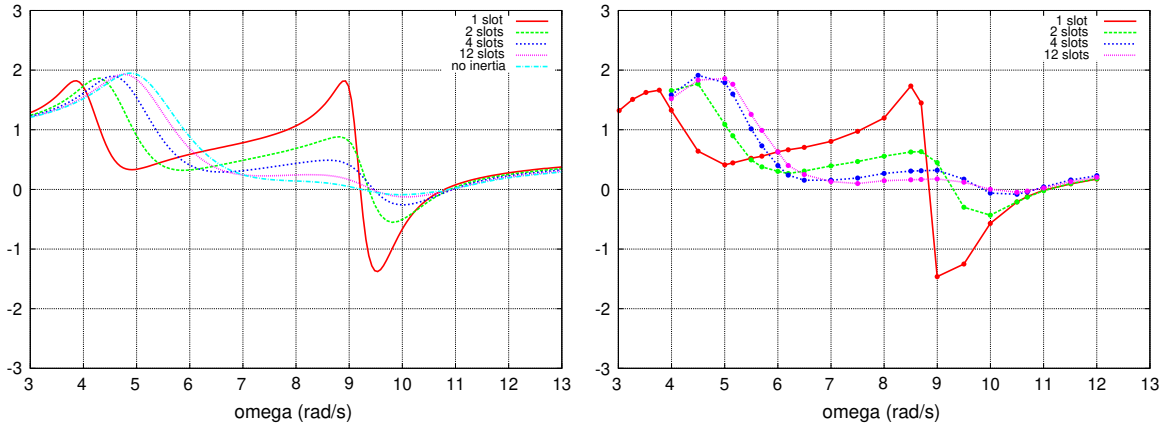

Fig. 6. Slatted screens. Added mass coefficient. Forced motion amplitude 4 mm. Calculated (left) and measured (right) values.

The inner length of the tank is 80 cm and the width 50 cm. The water-height was set to 32 cm during the tests, that is a waterdepth over tank length ratio h/B equal to 0.4, alike in our previous paper and in Faltinsen's et al. (2011a). The natural frequencies of the first three modes of the tank without screen (obtained from $\omega_n^2 = g\,\lambda_n \tanh \lambda_n h$, with $\lambda_n = n\pi/B$) are $\omega_1 = 5.72$ rad/s, $\omega_2 = 8.72$ rad/s and $\omega_3 = 10.74$ rad/s. The tests were run at angular frequencies from 3 rad/s through 12 rad/s, encompassing the frequencies of the first three modes, and at amplitudes of 1 mm, 4 mm, 8 mm and 12 mm.

In the tests with 12 or 4 vertical slots, alike in the previous tests with the circular openings, the tank was subdivided, lengthwise, into 4 compartments, with the double purpose of increasing the screen stiffness and of avoiding three-dimensional instabilities. In the tests with two slots, the number of compartments was reduced to two. In the one slot case, there was only one compartment and the plate thickness was increased to 4 mm to maintain rigidity. Fig. 3 shows the different slatted screens tested.

Fig. 4 shows the screens with circular openings. The plate thickness was 4 mm in all cases, with the tank divided into two compartments in the 36 holes and 18 holes cases. The mean free surface level can be seen in the photographs due to slightly different colors of the submerged and aerial parts. In the single hole case, the opening was set exactly, somewhat arbitrarily, at mid-way from the bottom to the free surface.

In all screen cases the porosity, or open-area ratio, is set at the same value of 18%, alike in Molin and Remy (2013).

4. Comparison between experimental and numerical results

4.1. Slatted screens

Figs. 5–8 show the added mass coefficients, from computations (left column), and from the tests (right column). Likewise Figs. 9–12 show the damping coefficients. Each figure is for a given motion amplitude, and shows results for the 4 types of

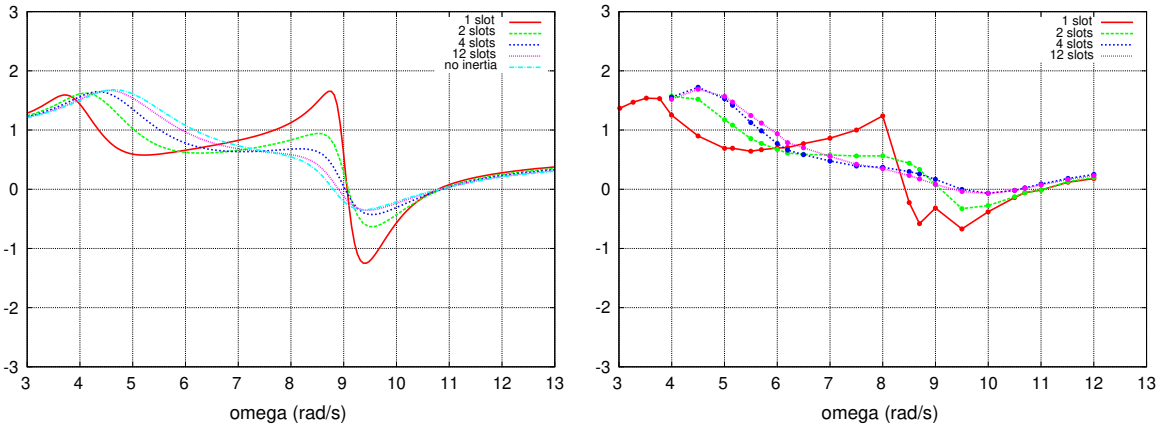

Fig. 7. Slatted screens. Added mass coefficient. Forced motion amplitude 8 mm. Calculated (left) and measured (right) values.

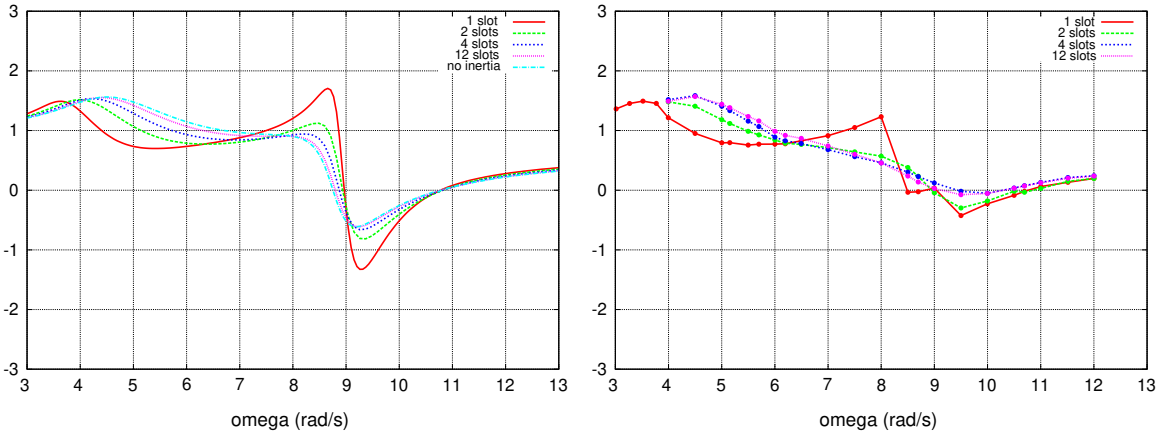

Fig. 8. Slatted screens. Added mass coefficient. Forced motion amplitude 12 mm. Calculated (left) and measured (right) values.

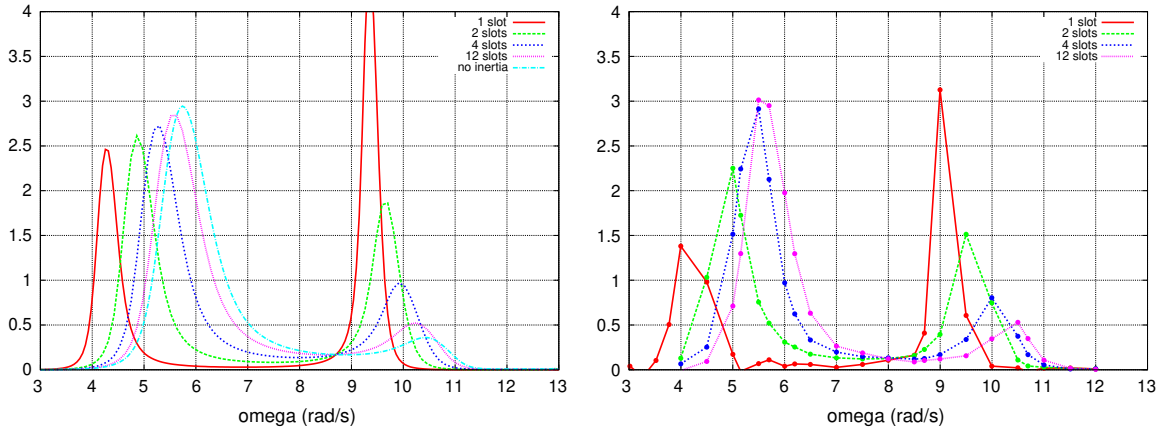

Fig. 9. Slatted screens. Damping coefficient. Forced motion amplitude 1 mm. Calculated (left) and measured (right) values.

screens. In the calculations, the hydrodynamic coefficients obtained with the initial discharge equation (1) (with no inertia term) are also shown.

As the number of slots is reduced the natural frequencies of the odd modes (ω_1 and ω_3) gradually decrease. This is in agreement with the findings of Faltinsen and Timokha (2009, 2011) in the case of a two-dimensional rectangular tank with horizontal slats. Table 1 shows calculated values; they were obtained by running the numerical code with a very small amplitude (0.01 mm), the damping coefficient then shows very sharp peaks at the natural frequencies. On the other hand the natural frequency of the second mode does not change. As a result, as inertia effects increase, ω_3 gets closer and closer to

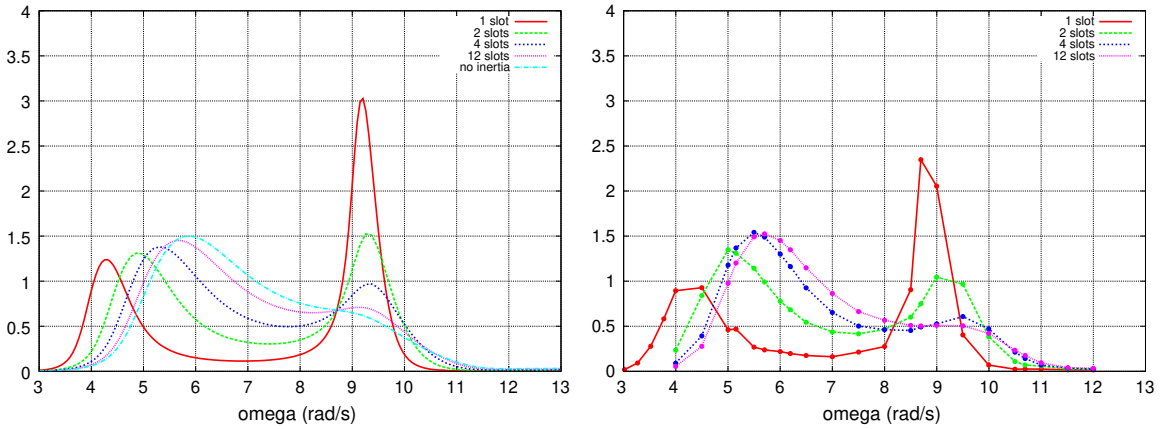

Fig. 10. Slatted screens. Damping coefficient. Forced motion amplitude 4 mm. Calculated (left) and measured (right) values.

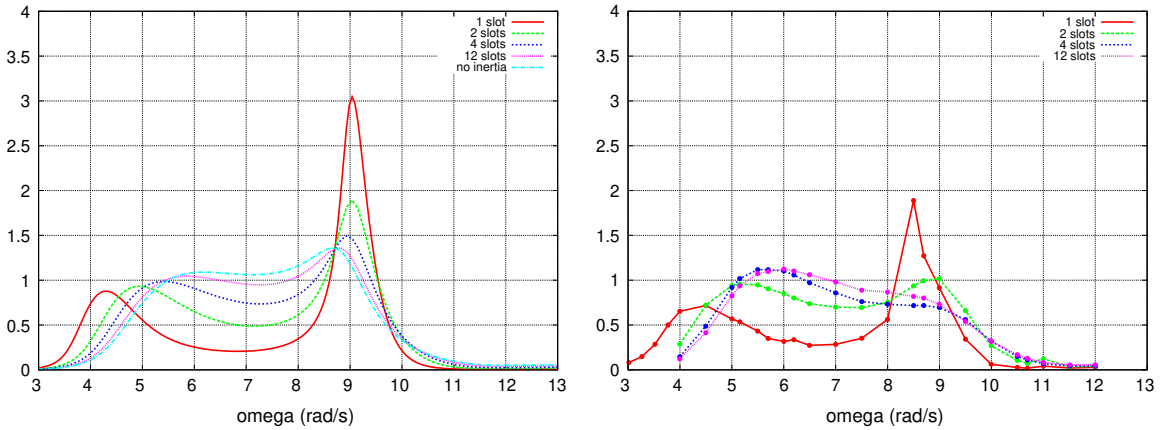

Fig. 11. Slatted screens. Damping coefficient. Forced motion amplitude 8 mm. Calculated (left) and measured (right) values.

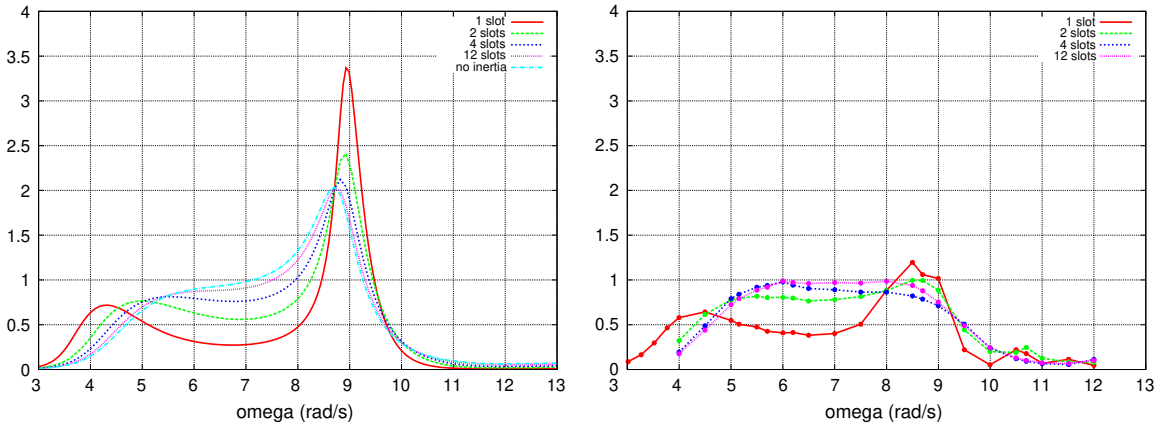

Fig. 12. Slatted screens. Damping coefficient. Forced motion amplitude 12 mm. Calculated (left) and measured (right) values.

ω_2. This might be a reason why the damping coefficient shows higher and higher peaks at a frequency in-between ω_2 and ω_3. On the other hand the damping coefficient decreases in the range $[\omega_1,\ \omega_2]$. It is remarkable that, at a given motion amplitude, the numerical damping curves exactly intersect at ω_2, and that the values obtained there are proportional to the motion amplitude.

At 1 mm and 4 mm motion amplitude, a generally good agreement is observed between numerical and experimental coefficients, with the experimental shifts of ω_1 and ω_3 correctly predicted by the numerical model. At larger amplitudes large discrepancies appear in the high frequency range, around ω_2 and ω_3 with the experimental damping peak being much

Table 1
Slatted screens. Calculated natural frequencies of modes 1 and 3.

Number of slots	ω_1 (rad/s)	ω_3 (rad/s)
1	4.28	9.42
2	4.86	9.80
4	5.25	10.16
12	5.54	10.52
No screen	5.72	10.74

Table 2
Screens with circular openings. Calculated natural frequencies of modes 1 and 3.

Number of openings	Radius (mm)	ω_1 (rad/s)	ω_3 (rad/s)
1	96	4.38	9.48
4	48	4.94	9.86
18	23	5.32	10.23
36	16	5.43	10.37
$\sim$ 2300	2	5.69	10.69
No screen		5.72	10.74

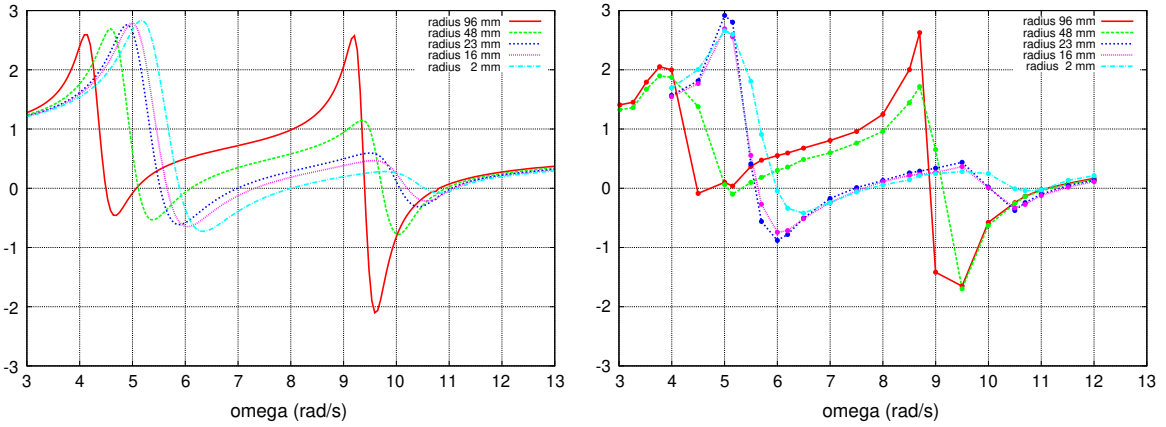

Fig. 13. Circular openings. Added mass coefficient. Forced motion amplitude 1 mm. Calculated (left) and measured (right) values.

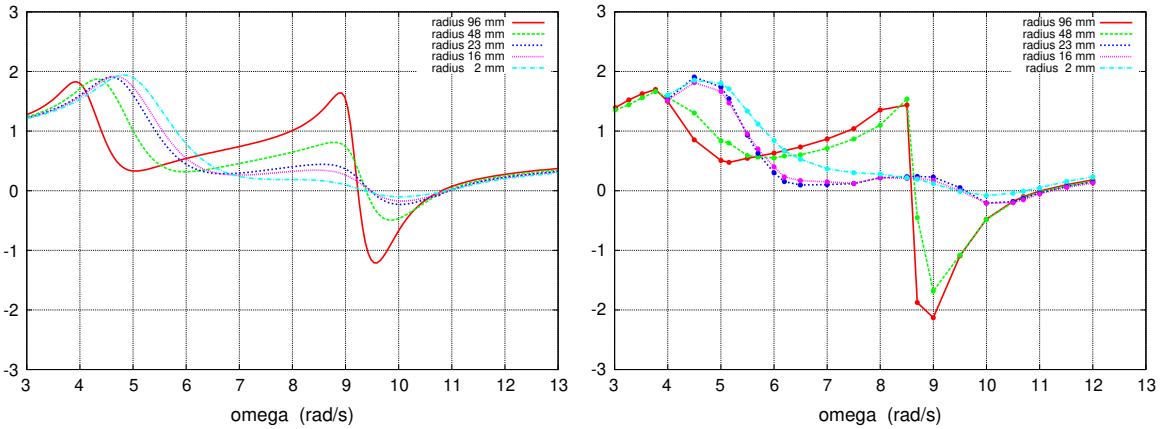

Fig. 14. Circular openings. Added mass coefficient. Forced motion amplitude 4 mm. Calculated (left) and measured (right) values.

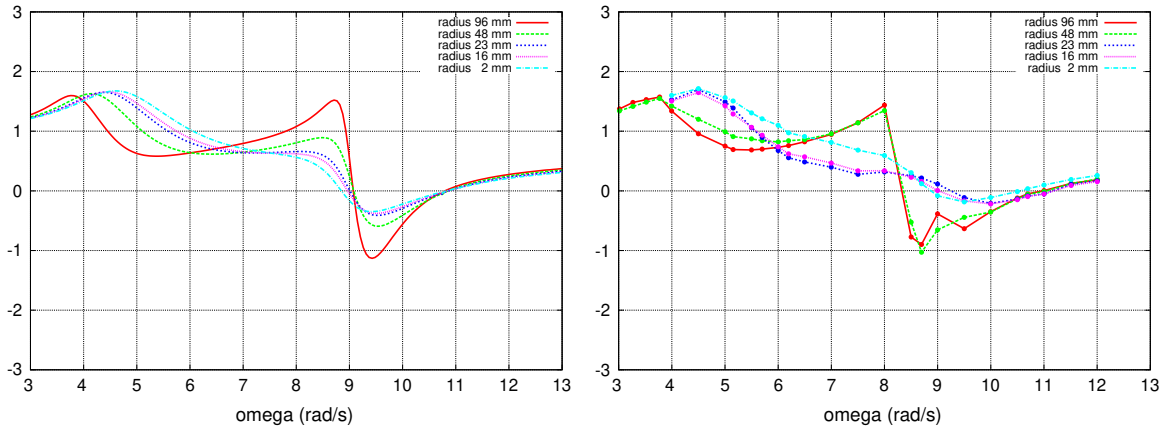

Fig. 15. Circular openings. Added mass coefficient. Forced motion amplitude 8 mm. Calculated (left) and measured (right) values.

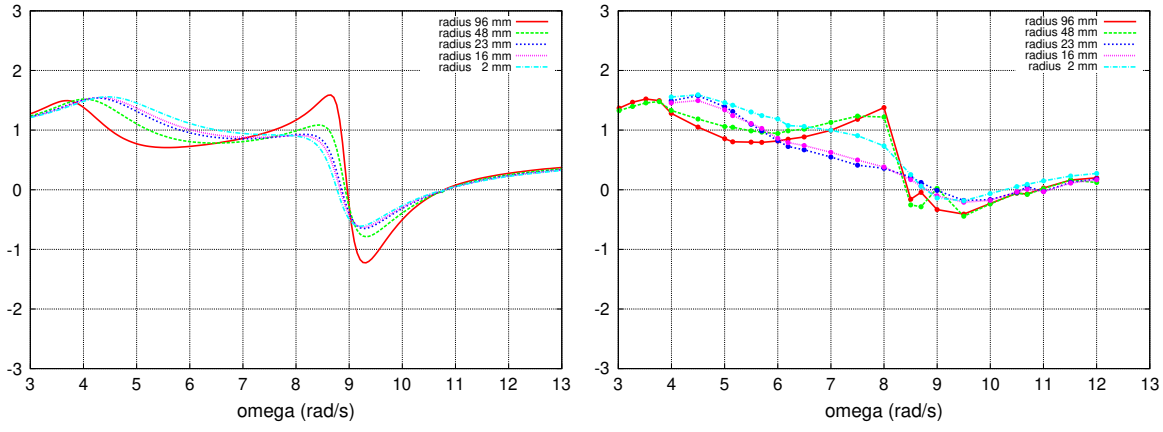

Fig. 16. Circular openings. Added mass coefficient. Forced motion amplitude 12 mm. Calculated (left) and measured (right) values.

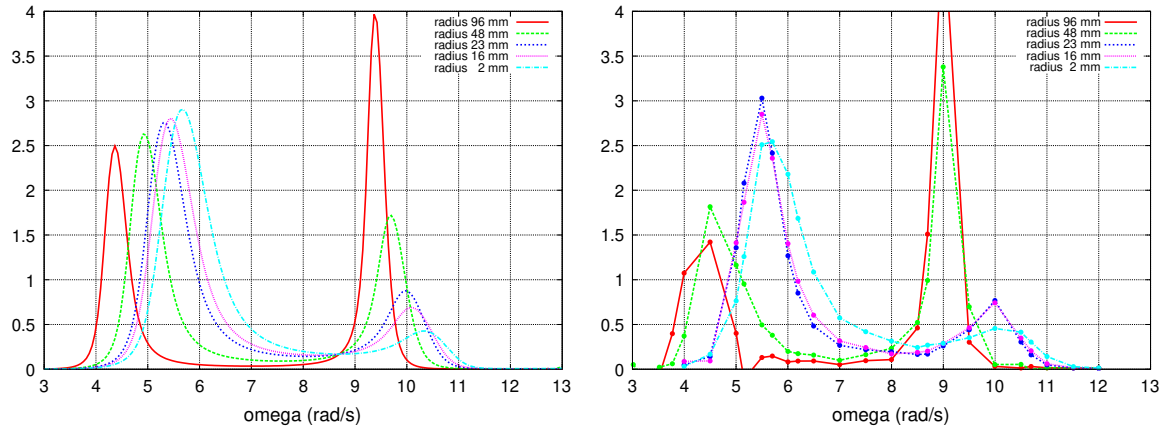

Fig. 17. Circular openings. Damping coefficient. Forced motion amplitude 1 mm. Calculated (left) and measured (right) values.

lower than the numerical one. As previously observed and commented in Molin and Remy (2013) this is due to nonlinear free surface effects, i.e. wave breaking which was observed in the tests, violating the linearity assumption of the free surface condition. Similar findings have been reported in Faltinsen et al. (2011b).

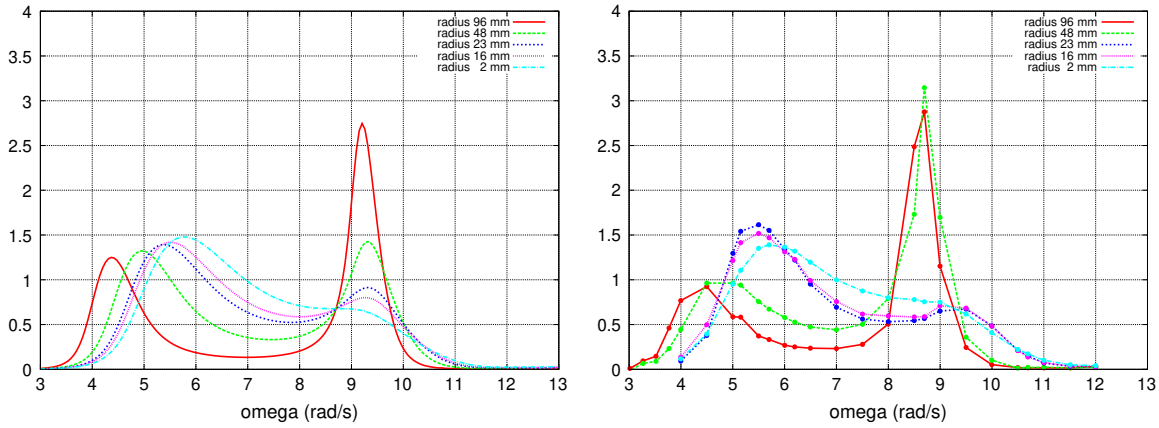

Fig. 18. Circular openings. Damping coefficient. Forced motion amplitude 4 mm. Calculated (left) and measured (right) values.

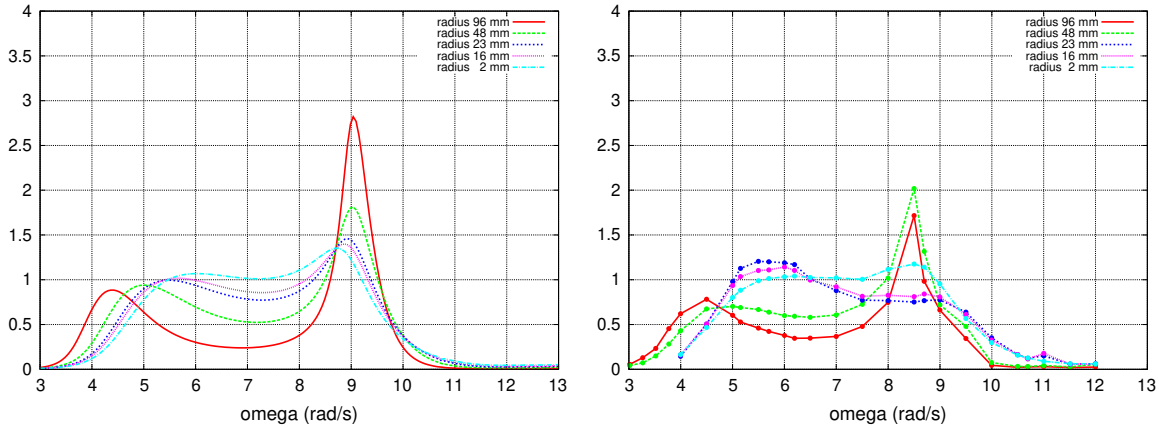

Fig. 19. Circular openings. Damping coefficient. Forced motion amplitude 8 mm. Calculated (left) and measured (right) values.

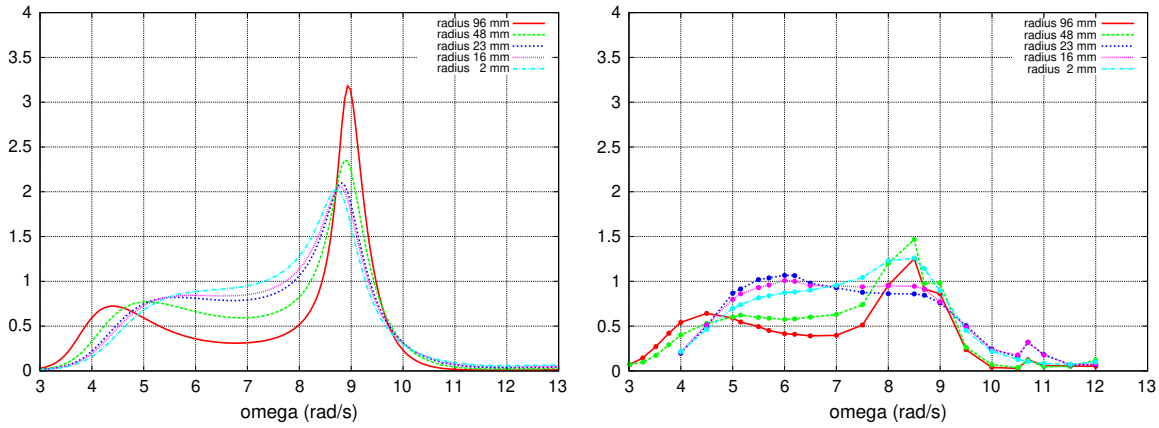

Fig. 20. Circular openings. Damping coefficient. Forced motion amplitude 12 mm. Calculated (left) and measured (right) values.

4.2. Screens with circular openings

Table 2 and Figs. 13–20 present the analogous results with the slatted screens, that is natural frequencies, added mass and damping coefficients. The 2 mm radius data have been taken from Molin and Remy (2013). From Tables 1 and 2 the natural frequencies are about the same for the two types of screen (if we associate the single slot and single opening cases,

the 2 slots' and 4 openings' cases, etc.), so the calculated values of the added mass and damping coefficients are also very similar. As for the experimental results, the agreement with calculated values is globally less good than in the slatted screens' case. For instance the downshift of the frequency ω_3 is a bit larger experimentally than numerically. As a result the experimental damping coefficients for the two larger openings at 1 mm and 4 mm forced motion amplitudes are larger than the numerical ones in the range $[\omega_2,\ \omega_3]$. On the other hand, in the smaller openings' cases, the experimental downshift is less than computed. These discrepancies might be due to ill estimation of the inertia effects with our model of a diaphragm in a circular duct. It is also expected that the location of the openings, with respect to the free surface, matters somewhat.

5. Discussion

In this paper we have proposed an extension of the discharge formula of Molin and Remy (2013) including an inertia term. This is similar to the Morison equation which combines a quadratic drag term with a linear inertia term. It proceeds from the same approach, combining two a priori contradictory fluid idealizations (viscous and non-viscous), but, when properly adjusted, providing results in reasonable agreement with measurements.

What sounds more uncertain in our model is to keep on idealizing the screen as a porous boundary of constant porosity all over the cross section, keeping the problem two-dimensional, when the openings become of a size comparable with the tank dimensions. It is also questionable whether we can keep on assuming that the flow in the tank can be modeled through potential flow theory. In Molin (2011) it is argued that, when the openings are infinitely small and numerous, the wakes remain confined within a thin distance from the screen and that a "clean" flow is recovered beyond. Obviously when the openings become comparable in size with the tank dimensions, this argument becomes weaker.

It is therefore a somewhat unexpected and fortunate result that our simple numerical model performs nearly as well with just a few openings as it does with the multiply perforated screens.

From the tests and computations, it appears that the main effect of decreasing the number of openings is to shift the resonant frequencies of the odd modes toward lower values. Since the natural frequencies of the even modes do not change (for a single screen set at mid-tank), the natural frequency of the third mode gets closer and closer to the second one. As a result the damping coefficient gets enhanced in this frequency range. Conversely it strongly decreases in the frequency range in-between the first and second modes.

TLDs are usually tuned so that the natural frequency of the first sloshing mode coincides with the target natural frequency of the system. Decreasing the number of openings may then be a way to reach the target frequency with a tank of moderate size.

All the results presented here are for a single porosity of 18%. In Molin and Remy (2013) it was argued that a relevant parameter is a combination of porosity and motion amplitude under the form $A\,(1-\tau)/(\mu\tau^2 B)$ and that it is therefore equivalent to vary τ or A (as long as linearized potential flow theory remains valid). When inertia effects come into play this statement is no longer valid. It is our intention to explore other porosity cases in the near future.

Appendix A. Added mass of a diaphragm in a circular pipe

Let b be the radius of the pipe, a the radius of the restriction, of zero thickness (see Fig. 21). We look for a velocity potential $\varphi(R,z)$ that satisfies the following boundary value problem:

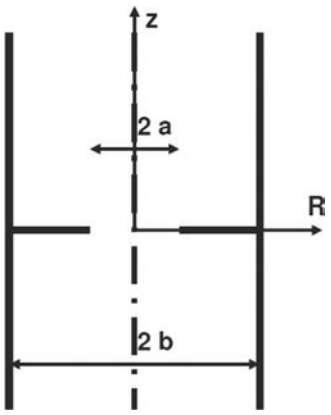

Fig. 21. Geometry.

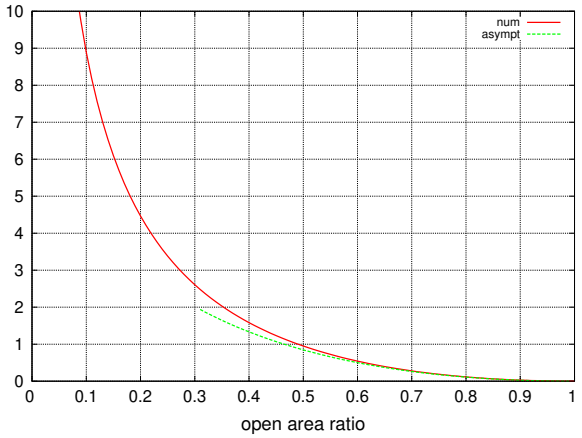

Fig. 22. Diaphragm in a circular pipe. Added mass coefficient vs open-area ratio.

$$\Delta\varphi = 0 \quad \text{fluid domain}, \tag{7}$$

$$\varphi_R = 0, \quad R = b, \tag{8}$$

$$\varphi_z = 1, \quad a \le R \le b; \ \ z = 0, \tag{9}$$

$$\varphi_z \to 0, \quad z \to \pm\infty. \tag{10}$$

In the upper sub-domain ($z \ge 0$), φ can be written as

$$\varphi_1 = A_0 + \sum_{n=1}^{\infty} A_n J_0(k_n R)\, \mathrm{e}^{-k_n z}, \tag{11}$$

where $k_n b$ are the roots of $J_0'(k_n b) = -J_1(k_n b) = 0$.

In the lower sub-domain, the velocity potential writes

$$\varphi_2 = -A_0 - \sum_{n=1}^{\infty} A_n J_0(k_n R)\, \mathrm{e}^{k_n z}. \tag{12}$$

With these expressions Eqs. (7), (8) and (10) are verified, together with the matching of the z-derivatives of φ_1 and φ_2 in $z=0$.

The conditions that remain to be fulfilled are

$$\varphi_1 = \varphi_2 = 0, \quad 0 \le R \le a; \ \ z = 0, \tag{13}$$

$$\varphi_{1z} = \varphi_{2z} = 1, \quad a \le R \le b; \ \ z = 0. \tag{14}$$

That is

$$A_0 + \sum_{n=1}^{\infty} A_n J_0(k_n R) = 0, \quad 0 \le R \le a, \tag{15}$$

$$\sum_{n=1}^{\infty} k_n A_n J_0(k_n R) = -1, \quad a \le R \le b. \tag{16}$$

Taking advantage of the orthogonality of the $J_0(k_n R)$ functions over [0 b], this can be transformed into the linear system:

$$k_0 a A_0 - 2\sum_{n=1}^{\infty} \frac{k_n - k_0}{k_n} A_n J_1(k_n a) = \frac{a^2 - b^2}{a}, \tag{17}$$

and, for $m = 1, \infty$:

$$k_m a A_0 J_1(k_m a) + \frac{k_m^2 b^2}{2} A_m J_0^2(k_m b) + \sum_{\substack{n=1 \\ n \ne m}}^{\infty} \frac{k_m a}{k_m + k_n} A_n \left[k_m J_1(k_m a) J_0(k_n a) - k_n J_0(k_m a) J_1(k_n a)\right] = a J_1(k_m a). \tag{18}$$

The series is truncated at some finite order M (M=400 for the results shown here) and the linear system is solved with a Gauss routine. In Eq. (17), k_0 is given an arbitrary value.

Fig. 22 shows the added mass coefficient $C_a = M_a/(\rho b^3) = -2\pi A_0/b$ obtained, as a function of the open area ratio a^2/b^2. Also shown in the figure is the asymptotic value of C_a for large values of a^2/b^2, that is $C_a = \pi^2\ (1-a/b)^2$.

References

Bennett, G.S., McIver, P., Smallman, J.V., 1992. A mathematical model of a slotted wavescreen breakwater. Coastal Engineering 18, 231–249.

Crowley, S., Porter, R., 2012a. The effect of slatted screens on waves. Journal of Engineering Mathematics 76, 53–76.

Crowley, S., Porter, R., 2012b. An analysis of screen arrangements for a tuned liquid damper. Journal of Fluids and Structures 34, 291–309.

Faltinsen, O., Firoozkoohi, R., Timokha, A.N., 2011a. Steady-state liquid sloshing in a rectangular tank with a slat-type screen in the middle: quasilinear modal analysis and experiments. Physics of Fluids 23, 042101.

Faltinsen, O., Firoozkoohi, R., Timokha, A.N., 2011b. Effect of central slotted screen with a high solidity ratio on the secondary resonance phenomenon for liquid sloshing in a rectangular tank. Physics of Fluids 23, 062106.

Faltinsen, O., Timokha, A.N., 2009. Sloshing. Cambridge University Press, New York, USA.

Faltinsen, O., Timokha, A.N., 2011. Natural sloshing frequencies and modes in a rectangular tank with a slat-type screen. Journal of Sound and Vibration 330, 1490–1503.

Mei, C.C., 1983. The Applied Dynamics of Ocean Surface Waves. Wiley-Interscience, New York, USA.

Molin, B., 2011. Hydrodynamic modeling of perforated structures. Applied Ocean Research 33, 1–11.

Molin, F., Remy, 2013. Experimental and numerical study of the sloshing motion in a rectangular tank with a perforated screen. Journal of Fluids and Structures 43, 463–480.

Morse, P.M., Ingard, K.U., 1968. Theoretical Acoustics. McGraw-Hill, New-York.

Tait, M.J., 2008. Modelling and preliminary design of a structure-TLD system. Engineering Structures 30, 2644–2655.